Letter

Competition between charge transfer and energy transfer: Influence of intrinsic defects in ZnO nanocrystals on rhodamine-B dye color signals

Seda Gürgen Avsar,[1] Sergej Repp,[2] Lisa Dietel,[2] Ahmet Güngör,[3] Stefan Weber,[2] Kasim Ocakoglu,[4] Shankari Nadupalli,[5,*] and Emre Erdem[3,†]

[1]*Department of Metallurgical and Materials Engineering, Faculty of Technology, Gazi University, 06500 Ankara, Turkey*
[2]*Institut für Physikalische Chemie, Albert-Ludwigs-Universität Freiburg, Albertstrasse 21, 79104 Freiburg, Germany*
[3]*Faculty of Engineering and Natural Sciences, Sabanci University, Istanbul 34956, Turkey*
[4]*Department of Engineering Sciences, Faculty of Engineering, Tarsus University, TR-33400 Tarsus, Turkey*
[5]*Department of Materials Science and Engineering, Faculty of Engineering, Tel Aviv University, 6997801 Israel*

(Received 3 October 2023; revised 14 November 2023; accepted 17 November 2023; published 6 December 2023; corrected 3 January 2024)

The complexity of the competition between nonradiative energy transfer and charge transfer is presented in this work. This study uses ZnO nanocrystals as a donor component and rhodamine B (RhB) dye as an acceptor component. Investigations reveal that the concentration of intrinsic defects and their localization, particularly oxygen vacancies, zinc interstitials, and oxygen interstitials, play a vital role in nonradiative energy transfer from ZnO nanocrystals to RhB dye. Additionally, photoluminescent spectra indicate that ZnO nanocrystals degrade the emission signals of RhB dye via charge transfer. It is possible that a part of oxygen vacancies may also contribute to the photocatalytic oxidation of the RhB molecule. The correlation between electron paramagnetic resonance, photoluminescence, and the RhB emission decay rates indicates two processes that one may encounter when dealing with semiconductor-dye conjugates. First is a complex energy transfer from ZnO to RhB indicating a photoluminescent up-conversion and second is a charge transfer from photoexcited intrinsic defect species in ZnO suppressing the RhB emission signals, which occur together. The defect species involved in photoluminescent up-conversion in ZnO+RhB is due to a nonradiative energy transfer from photoexcited zinc interstitials or doubly charged oxygen vacancies in ZnO to RhB. Additionally, the suppression of RhB emission occurs due to charge transfer from oxygen vacancies in ZnO.

DOI: 10.1103/PhysRevB.108.L241401

I. ENERGY TRANSFER AND CHARGE TRANSFER

Förster resonance energy transfer (FRET) involves a process where a photoexcited donor transfers energy nonradiatively to an acceptor fluorophore. The particulars of the FRET phenomenon are illustrated in Fig. 1. Both donor and acceptor components emit photons of a selected wavelength after absorbing photons with energies that correspond to the electronic structure of the individual components. For FRET interaction to occur, it is essential that (i) the energy of the donor emission overlaps with the absorption energy of the acceptor [illustrated in Fig. 1(a)] and (ii) the donor component and the acceptor component should be in close proximity to each other (1–10 nm). When both of these requirements are fulfilled, photonic energy absorbed by the donor component is transferred nonradiatively to the acceptor component, resulting in a radiative emission from the acceptor component at a selected wavelength. This phenomenon is an excellent tool to determine the location of two components and the interaction or noninteraction between them [as shown in Fig. 1(b), right].

The FRET phenomenon is applied in a wide variety of devices with a significant maturity in biomedical [1], biosensing (as an indicator of successful functionalization of molecules) [2–5], environmental sciences, signal enhancement in florescence imaging, and surface enhanced Raman scattering (SERS) [6]. The ability to tag and untag a variety of dye molecules to polar metal oxides such as zinc oxide (ZnO) leads to various applications in devices such as photodetectors, photovoltaic energy converters, whispering gallery mode lasers (lasing upon binding) [7], cell tagging, intracellular sensing and signaling, imaging, water effluent degradation [8–14], biocontrolled photonic devices such as enzyme linked immunosorbent assay (ELISA) [15,16], and photocatalytic devices. Several wide band-gap metal oxides are used in making sensor devices that work on FRET. Our previous set of works cover a wide range of applications and investigate the localization of intrinsic defect species in ZnO nanocrystals [17–21]. It is also known that the photocatalytic activity of metal oxides is influenced by the size, structure, defects, and dopants in the metal oxides [10]. Although there are studies that cover the influence of size and morphology on the photocatalytic activity [14,22–28], few studies present the competition between FRET and photocatalytic activity [5], while both activities may be influenced by the localization and concentration of intrinsic defect species in the donor ZnO component.

One method to understand the influence of ZnO's local electronic structure on FRET and non-FRET is by asking

*shankari.nanotech@gmail.com
†emre.erdem@sabanciuniv.edu

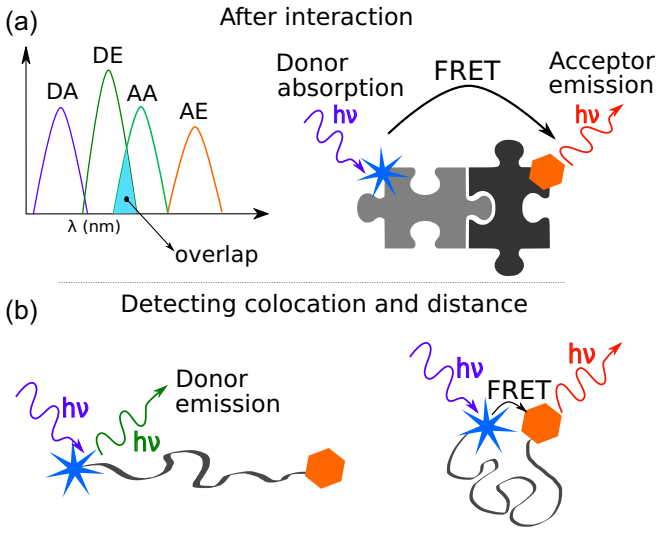

FIG. 1. (a) Gray puzzle pieces depict the donor component and black puzzle pieces represent an acceptor component. FRET phenomenon occurs only when the energy window of the donor component's emission signal (DE) overlaps (highlighted in blue) with that of the acceptor component (AA). Here DA, DE, AA, and AE represent energy windows of donor absorption, donor emission, acceptor absorption, and acceptor emission signals, respectively. (b) The advantage of FRET is visualized here. By detecting the wavelength or energy of the emission signals, one can detect interaction or noninteraction and the proximity between the donor and acceptor components. When the acceptor component is away, only donor emission signals are detected. When the donor and acceptor components are in close proximity, a signal with a wavelength that corresponds to the acceptor emission is detected.

the following questions. Does annealing metal oxides in an oxygen rich atmosphere affect the concentration of defect species and their localization? Which intrinsic defect species localize on the surface? Does the intrinsic defect carry along with it a hole or an electron to enable ease of transfer [17,29]? Do emission and absorption regions of defects localizing on the surface of ZnO nanocrystals and the dye molecules overlap to enable nonradiative charge transfer [14,30,31]? If yes, then does the energy from the overlap transfer entirely to the acceptor, thereby enhancing the emission signal proportionally? Do defect induced charge species take part simultaneously in photocatalytic oxidation of the acceptor dye molecule?

This study intends to provide observational insight into the questions presented above while presenting quantitative information on the influence of intrinsic defect species on photoinduced energy transfer and/or photocatalytic activity.

II. METHODS AND CHARACTERIZATION TECHNIQUES

A. Sample preparation

In this study, zinc nitrate hexahydrate $Zn(NO_3)_2 \cdot 6H_2O$, Alfa Aeser, Germany, ammonium hydroxide (NH_4OH, Sigma Aldrich, Germany), soluble starch powders [$(C_6H_{10}O_5)_n$, Sigma Aldrich, Germany], absolute ethanol (Sigma Aldrich, Germany), and rhodamine B ($C_{28}H_{31}ClN_2O_3$, Merck, Germany) are used. A starch solution is prepared by mixing 5 g of soluble starch to 150 ml deionized water at room temperature. This solution is stirred for 60 min on a heating plate. To this starch solution, 0.01 mol $Zn(NO_3)_2 \cdot 6H_2O$ is added and stirred at 85 °C for 30 min. The resulting precipitate is centrifuged, washed with deionized water, and dried overnight at 50 °C. The obtained powders are calcinated at 100, 200, 300, 400, 500, 600, and 700 °C, respectively, in air to obtain a variation of ZnO crystalline sizes. A separate dye solution is prepared by mixing 0.001 M absolute ethanol and rhodamine B. This dye solution is mixed with ZnO powders by stirring for 12 h in a dark enclosure.

B. Characterization techniques

X-ray powder diffraction patterns are collected with a Bruker D8 Advanced Series powder diffractometer (40 kV, 40 mA, CuKα radiation, $\lambda = 1.5405$ Å) at ambient temperature in steps of 0.03° in the range $20° \leqslant 2\theta \leqslant 80°$.

The morphology and size of the ZnO crystals are obtained using a Transmission Electron Microscope (TEM) 912, Model - Zeiss LEO 912 Omega, instrument with an electron acceleration voltage of 120 kV. Samples for the TEM are prepared by evaporating a dilute suspension of particles onto a carbon-coated copper grid. X-band (9.8 GHz) electron paramagnetic resonance (EPR) measurements are performed on Bruker EMX spectrometer using a rectangular TE102 resonator. Every sample is measured at 2 mW microwave power modulation amplitude and 100 kHz modulation frequency. Data processing is carried out with the software WIN-EPR (Bruker). Photoluminescence spectra are recorded with a Perkin-Elmer LS 55 fluorescence spectrometer with 325 nm excitation wavelength and 5 nm excitation and emission slit width. A pulsed Xenon lamp is used as the excitation source. To remove spurious emission from the source, a UG 5 filter is used. The UV-VIS spectrum is obtained from a Shimadzu UV-2450 UV-VIS spectrometer with a measuring wavelength range 190–900 nm with 0.1 nm resolution at room temperature. Data processing is carried out with the software UVPROBE.

III. OBSERVATIONS AND DISCUSSIONS

The x-ray diffractograms of uncalcinated ZnO crystals and those calcinated at various temperatures (100 °C to 700 °C) are given in Fig. 2(a). The peaks of the diffraction lines for all the samples overlap and align with the fingerprint ZnO wurtzite structure [17]. A small shift in the centers of the diffraction peaks is observed with change in calcination temperature [shown in Fig. 2(b)]. This shift becomes negligible for ZnO crystals calcinated at temperatures above 400 °C. TEM images displayed in Fig. 2(c) show hexagonal platelike morphology. Images show that the size of the ZnO crystals ranges from 60 to 150 nm for samples calcinated at 500 °C and 700 °C.

X-band EPR spectroscopy results for ZnO crystals uncalcinated and calcinated at temperatures 200 °C to 600 °C are given in Fig. 2(d). For crystals calcinated at $\geqslant$ 600 °C, a single line at $g = 1.96$ is observed [32–34]. For ZnO calcinated at 200 °C to 500 °C, an additional signal at $g = 2.004$ is observed, along with the signal at $g = 1.96$. From

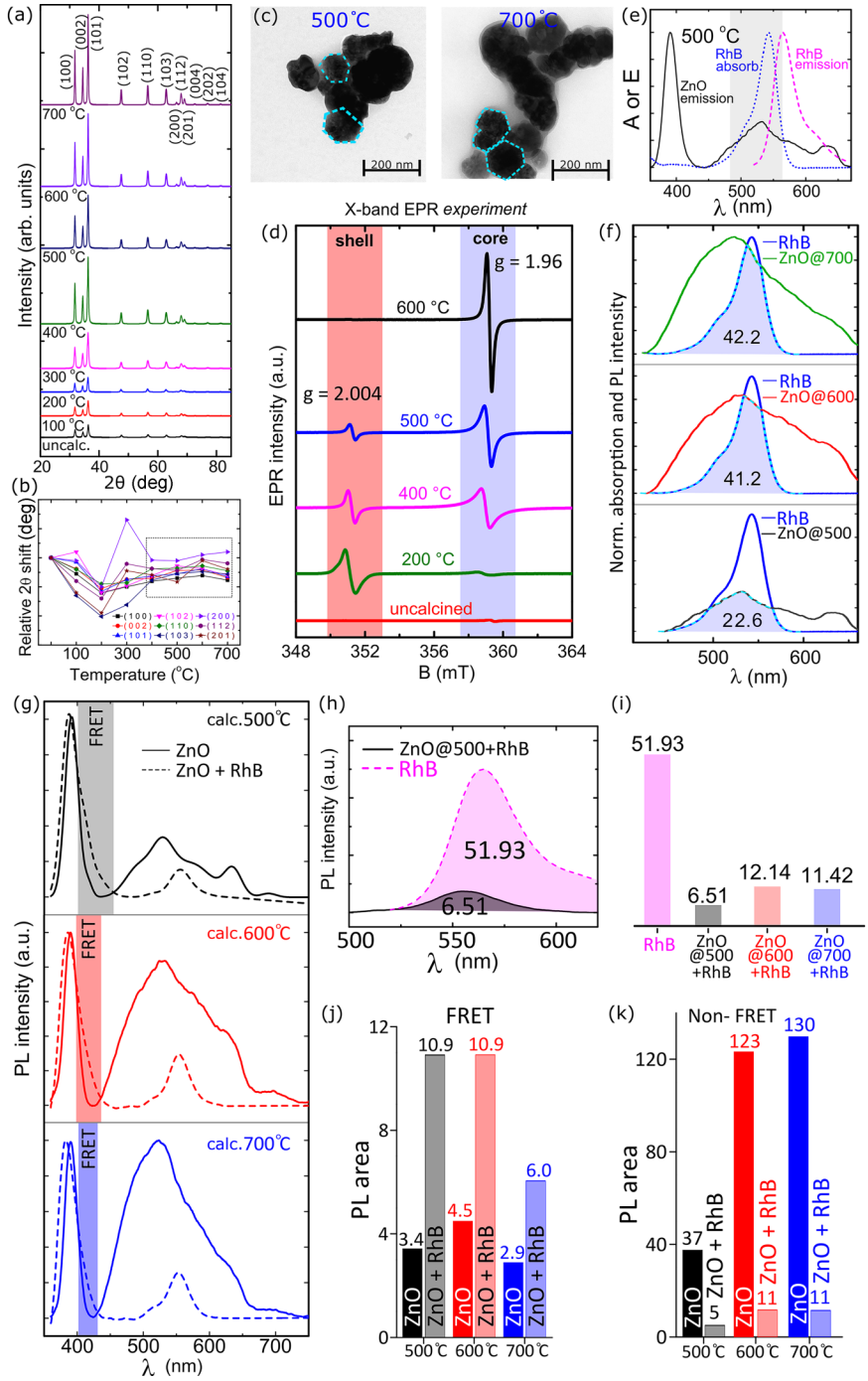

FIG. 2. (a) X-ray diffraction lines for uncalcinated and calcinated ZnO samples at various temperatures. (b) Relative 2theta shift of x-ray diffraction (XRD) peaks in comparison to the uncalcinated sample. (c) TEM images for ZnO particles calcinated at 500 °C and 700 °C. A typical hexagonal (trigonal symmetry of ZnO) platelike morphology is observed. (d) EPR spectral lines for ZnO particles calcinated at various temperatures in comparison to the uncalcinated sample. For crystals calcinated at and above 600 °C, a single sharp line at $g = 1.96$ is observed. For ZnO crystals calcinated below 500 °C, a faint signal at $g = 2.004$ develops. This signal is attributed to the oxygen vacancies (V_O). (e) Shows the fundamental requirement for FRET to occur, i.e., for a nonradiative energy transfer between ZnO to RhB, the donor (ZnO) emission signal should overlap (areas shaded gray) with the acceptor (RhB) absorption signal. (f) Photoluminescence (PL) emission lines for ZnO particles calcinated at 700 °C (in green), 600 °C (in red), and 500 °C (in black) along with the absorption spectra of RhB dye. The area shaded blue in (f) is the overlap region between ZnO's emission and RhB absorption signals. The numbers given in the shaded region represent the area of the overlap region. (g) PL spectra of ZnO and ZnO+RhB at various calcination temperatures. (h) Visualization of quenching of RhB's emission signal when ZnO is mixed with RhB. Numbers represent the area under the PL peak. (i) Comparison of the RhB emission signals with emission signals of RhB+ZnO annealed at 500 °C, 600 °C, and 700 °C. (j) Area under the emission signals of RhB+ZnO (annealed at various temperatures) that resulted from FRET in comparison to emission signals of just ZnO at the same energy window. (k) PL areas that represent electron transfers.

previous studies, the signal at $g = 1.96$ is attributed to intrinsic defects such as Zn vacancies (V_{Zn}), whereas the signal at $g = 2.004$ is attributed to the oxygen vacancies (V_O) that localize on the surface or shell of the particle [17,20,21,35]. For this reason, from here on, the EPR line at $g = 1.96$ is called the core signal, and the line at $g = 2.004$ is called a shell signal. TEM images show that samples calcinated at 500 °C have a distribution of nanocrystals (50–100 nm) leading to a prominent shell signal in EPR, whereas the samples calcinated at 600 °C and above,have a larger distribution of particles in the range 100–150 nm, leading to an individual core EPR signal. The area under the integrated line of each EPR signal gives a direct estimate of the concentration of the defects being observed. The concentration of core (C) defects for the ZnO crystal calcinated at 200, 400, 500, 600, and 700 is $C_{200} = 1.7 \times 10^5$, $C_{400} = 4.1 \times 10^5$, $C_{500} = 1.4 \times 10^6$, $C_{600} = 1.1 \times 10^6$, and $C_{700} = 1.7 \times 10^6$, respectively, and the concentration of shell (S) defects is $S_{200} = 1.3 \times 10^6$, $S_{400} = 2.6 \times 10^6$, $S_{500} = 1.8 \times 10^5$, and $S_{600} =$ negligible. Hence, annealing ZnO crystals at higher temperatures in an ambient atmosphere leads to less or negligible V_O defect species.

A detailed investigation on photoluminescence (PL) emission signals and their relation to intrinsic defect species is covered in our previous work [17]. The green (in the $\lambda = 520$ nm or 2.38 eV region) PL signal is attributed to V_O [36]. Figure 2(e) shows the overlap (highlighted in gray) between ZnO emission and rhodamine B dye (RhB) absorption (the plot is given for ZnO annealed at 500 °C), which is essential for FRET to occur. Figure 2(e) also shows RhB emission signal range. Figure 2(f) shows the PL emission for samples of ZnO (annealed at 500 °C in black, 600 °C in red, and 700 °C in blue). The region shaded in blue in Fig. 2(f) shows the overlap integral between ZnO PL emission signals and RhB absorption spectra. The area ($A^{\text{Temp.}}_{\text{overlap}}$) for ZnO nanocrystals is $A^{500}_{\text{overlap}} = 22.6$, $A^{600}_{\text{overlap}} = 41.2$, and $A^{700}_{\text{overlap}} = 42.2$. These results show that ZnO nanocrystals with a higher concentration of shell defects (annealed at 500 °C) has a smaller overlap when compared to those with a lower concentration of shell defects (ZnO annealed at 600 °C and 700 °C).

At this point, it is necessary for any study claiming to have a FRET phenomenon involved to refer to the analysis conducted by Moroz *et al.* [5]. Moroz *et al.* state that (i) most studies presenting FRET efficiency analyze the PL intensity of the donor before and after tagging it to the acceptor. This PL intensity difference is used to quantitatively estimate the nonradiative photoinduced energy that is transferred from the donor to acceptor. (ii) However, one must not rule out the non-FRET contributions, such as electron transfer or exciton mediated transfer. To detect non-FRET contributions, one should monitor the change in the total charge of donor and acceptor components during photoexcitation [5].

The current study intends to assess the contribution defect localization in the donor component on the emission signals of the donor + acceptor component. This study uses the following steps to assess FRET and non-FRET contributions. (i) Using the spin-counting method on EPR spectra, one can extract information about defect localization and, indirectly, the charge profile of the ZnO nanocrystals. (ii) The PL spectra of the donor and donor+acceptor provide information about emission signal regions that are either suppressed or enhanced. (iii) For non-FRET-based electron transfers, a correlation between the charge profile and suppressed PL emission signals should be observed. For FRET-based energy transfer, the PL emission signals for donor+acceptor should show an enhancement in certain selected regions when compared to just donor emission signals.

Figure 2(g) compares the emission signals of ZnO nanocrystals and those that are mixed with RhB. The first observation is a stark suppression of the emission signals above 450 nm for ZnO + RhB crystals. The second observation would be an enhanced emission signal for ZnO + RhB samples starting at ≈402 nm and ending at ≈450 nm when compared to ZnO nanocrystals. Figure 2(h) shows that the PL intensities of the RhB emission signals are drastically reduced and emissions above 580 nm are null when RhB is mixed with ZnO nanocrystals calcinated at 500 °C. Comparison of the areas under the PL spectra for this region is given in Fig. 2(i). The area under the emission spectra of the RhB dye molecule is $A_{\text{RhB}} = 51.93$. The areas $A^{\text{Temp.}}_{\text{ZnO+RhB}}$ of the PL spectral lines for ZnO+RhB are $A^{500}_{\text{ZnO+RhB}} = 6.51$, $A^{600}_{\text{ZnO+RhB}} = 12.14$, and $A^{700}_{\text{ZnO+RhB}} = 11.42$. From Fig. 2(h), it is clear that the RhB emission signal is both attenuated and certain wavelengths ($\geqslant$580 nm) are completely blocked. A suppression of the PL signal for the ZnO+RhB composite in the range $480 \leqslant \lambda \geqslant 620$ nm is representative of the concentration of RhB molecules that is oxidized due to charge transfer between the ZnO nanocrystals and RhB molecules. Furthermore, the area under the PL spectra for ZnO nanocrystals is compared with the PL spectra of the ZnO+RhB composite in the 405 to 450 nm region. An enhancement in the emission signals of the ZnO+RhB when compared to native ZnO or RhB's emission signals is considered FRET [FRET regions are highlighted in Fig. 2(g)] and the suppression of the PL signals may be considered as charge transfer from ZnO to RhB molecules.

This study reveals the complexity of FRET and non-FRET phenomena in such donor-acceptor composites. Additionally, FRET-based emission in the region 405–450 nm [as shown in Fig. 2(g)] can be attributed to features observed in sensitizer-emitter complexes where PL up-conversion occurs. Two possible photon up-conversion mechanisms such as (a) energy transfer up-conversion and (b) triplet-triplet annihilation up-conversion may occur either individually or simultaneously in RhB-ZnO complexes after initial excitation. The photon up-conversion may also include a vibrational relaxation or internal conversion between the energy levels attributed to intrinsic defect species, that is, from the conduction band to $V_O^{0/++}$, Zn_i, and O_i energy states inside the band gap, after which an intersystem crossing between the defect species and RhB may occur [37,38].

Two bar charts, one showing the area under the PL signals that indicate FRET [Fig. 2(j)] and the other showing non-FRET charge transfer [Fig. 2(k)] are given. ZnO nanocrystals annealed at 500 °C and 600 °C show quantitatively similar FRET phenomena. ZnO+RhB annealed at 500 °C enhance the emission signals in the $405 \leqslant \lambda \geqslant 455$ nm region by a greater extent than ZnO+RhB annealed

at 600 °C, as shown in Fig. 2(j). ZnO+RhB annealed at 700 °C shows a very bleak PL signal enhancement [Fig. 2(j)], but the same sample shows a larger suppression of the PL signal [ZnO+RhB at 700 °C in Fig. 2(k)], indicating that charge transfer dominates FRET in this sample. The values $\eta_{\mathrm{FRET}}^{\mathrm{anneal.temp.}} = (A_{\mathrm{ZnO+RhB}}^{\mathrm{FRET}} - A_{\mathrm{ZnO}}^{\mathrm{FRET}})/A_{\mathrm{ZnO-RhBemission}}^{\mathrm{overlap}}$ are $\eta_{\mathrm{FRET}}^{500} = 0.33$, $\eta_{\mathrm{FRET}}^{600} = 0.16$, and $\eta_{\mathrm{FRET}}^{700} = 0.07$. One must note that the definition of η here is not the usual FRET efficiency. The numerator gives a value that indicates the enhancement of the PL in a range of wavelengths where FRET is observed. The denominator is the area of overlap between the PL emission of ZnO and the absorption signals of RhB, which gives an estimate of the total energy transferred for FRET to occur in an ideal scenario. Its seems that ZnO nanocrystals annealed at 500 °C has the highest FRET efficiency compared to those annealed at other temperatures. Additionally, a higher green PL signal (520–540 nm) in ZnO nanocrystals correlates to the attenuation of all the PL signals above 455 nm when ZnO nanocrystals are mixed with RhB [see the PL intensities in Fig. 2(g) and look at the non-FRET bar chart in Fig. 2(k)]. This shows that the green PL signal, which is attributed to V_O defect species in ZnO [17], is responsible for electron transfer between the ZnO nanocrystal and RhB molecule. It is possible that photoexcitation from V_O to the conduction band or from V_O to a shallow defect center Zn_i may generate electron-hole pairs. These photogenerated holes (h^+) may promote direct or OH^- radial mediated photocatalytic oxidation of RhB dye molecules. Previous studies showed that the concentration of the defects, dissolution of ZnO + RhB in liquid media, and the light excitation wavelength and intensity will affect the attenuation of the dye emission signal [5,39–41].

Since we have information on the amount of defect species for ZnO nanocrystals from EPR, a correlation between the defect species and non-FRET dye signal quenching could be made. ZnO nanocrystals annealed at temperatures above 500 °C showed no prominent shell signal. However, the dye emission signals showed greater suppression for ZnO+RhB samples where ZnO nanocrystals are annealed at temperatures 600 °C and 700 °C.

On the other hand, Beane *et al.* showed FRET from a defect state, unlike most studies which show a transfer of excitonic energy between ZnO and A594 cadaverine, and proved that only surface adsorbed dyes can actively quench the defect emission signals [42]. Additionally, there are studies that indulge in understanding the charge transmission and charge transfer by polaron hopping where the rate of transfer depends on the media (such as orientation, symmetry, and media-molecule interaction) [29,43,44]. Hence this study cannot draw conclusions about the origin behind FRET and non-FRET with certainty. This study, however, shows that there can be a competition between FRET and charge transfer in semiconductor nanoparticles and dye conjugates.

Ideally, if only the FRET phenomenon occurs, photoexcitation from the band edge should trigger an energy transfer from the trapped state or from the defect states of ZnO to RhB, increasing the acceptor emission signal and consequently quenching the donor's emission signal. However, in cases where there is a competition between FRET and electron transfer, a successful transfer of energy might not result in a strong acceptor emission signal, rather a quenching of the defect state responsible for FRET is observed along with the suppression of the dye emission signal. If the energies of the defect state in ZnO responsible for FRET and the energy of the dye's emission signal have a small difference, a convoluted signal is obtained. Additionally, looking at the regions highlighted in the PL spectra [Fig. 2(g)], there is a possibility that novel emissions may arise due to energy transfer that do not correspond to the native emissions of the acceptor or donor. This study raises the following questions: To what do these low-energy emission signals that seem to arise from energy transfer correspond to? When amount of quenching of the donor emission signal does not correspond to the enhancement of the emission signals resulting from FRET, what happens to the energy that is transferred?

ACKNOWLEDGMENTS

E.E. and A.G. thank TÜBITAK for financial support for scientific Grants No. 118C243 and No. 121C416. S.N. is grateful for the postdoctoral fellowship from Tel Aviv University which supported her research endeavors.

E.E. designed the experiments and guided the scientific investigations. S.G.A. performed all the experiments and collected the required data. S.N. visualized, analyzed, and prepared the drafts of this Letter. All the authors contributed equally in discussing the observations of this investigation.

[1] X. Shen, W. Xu, J. Ouyang, and N. Na, Fluorescence resonance energy transfer-based nanomaterials for the sensing in biological systems, Chin. Chem. Lett. **33**, 4505 (2022).

[2] Z. Jin, N. Dridi, G. Palui, V. Palomo, J. V. Jokerst, P. E. Dawson, Q.-X. A. Sang, and H. Mattoussi, Quantum dot–peptide conjugates as energy transfer probes for sensing the proteolytic activity of matrix metalloproteinase-14, Anal. Chem. **95**, 2713 (2023).

[3] A. R. Clapp, I. L. Medintz, J. M. Mauro, B. R. Fisher, M. G. Bawendi, and H. Mattoussi, Fluorescence resonance energy transfer between quantum dot donors and dye-labeled protein acceptors, J. Am. Chem. Soc. **126**, 301 (2004).

[4] K. Boeneman, B. C. Mei, A. M. Dennis, G. Bao, J. R. Deschamps, H. Mattoussi, and I. L. Medintz, Sensing caspase 3 activity with quantum dot-fluorescent protein assemblies, J. Am. Chem. Soc. **131**, 3828 (2009).

[5] P. Moroz, Z. Jin, Y. Sugiyama, D. Lara, N. Razgoniaeva, M. Yang, N. Kholmicheva, D. Khon, H. Mattoussi, and M. Zamkov, Competition of charge and energy transfer processes in donor–acceptor fluorescence pairs: Calibrating the spectroscopic ruler, ACS Nano **12**, 5657 (2018).

[6] I. Marica, F. Nekvapil, M. Ştefan, C. Farcău, and A. Falamaş, Zinc oxide nanostructures for fluorescence and Raman signal enhancement: A review, Beilstein J. Nanotechnol. **13**, 472 (2022).

[7] N. Toropov, G. Cabello, M. P. Serrano, R. R. Gutha, M. Rafti, and F. Vollmer, Review of biosensing with whispering-gallery mode lasers, Light Sci. Appl. **10**, 42 (2021).
[8] M. Le Pivert, R. Poupart, M. Capochichi-Gnambodoe, N. Martin, and Y. Leprince-Wang, Direct growth of ZnO nanowires on civil engineering materials: Smart materials for supported photodegradation, Microsyst. Nanoeng. **5**, 57 (2019).
[9] N. Yadav, V. K. Garg, A. K. Chhillar, and J. S. Rana, Detection and remediation of pollutants to maintain ecosustainability employing nanotechnology: A review, Chemosphere **280**, 130792 (2021).
[10] M. Y. Guo, A. M. C. Ng, F. Liu, A. B. Djurisic, W. K. Chan, H. Su, and K. S. Wong, Effect of native defects on photocatalytic properties of ZnO, J. Phys. Chem. C **115**, 11095 (2011).
[11] Y. Lai, M. Meng, and Y. Yu, One-step synthesis, characterizations and mechanistic study of nanosheets-constructed fluffy ZnO and Ag/ZnO spheres used for Rhodamine B photodegradation, Appl. Catalys. B: Environ. **100**, 491 (2010).
[12] S. Baruah, S. S. Sinha, B. Ghosh, S. K. Pal, A. K. Raychaudhuri, and J. Dutta, Photoreactivity of ZnO nanoparticles in visible light: Effect of surface states on electron transfer reaction, J. Appl. Phys. **105**, 074308 (2009).
[13] A. Senthamizhan, B. Balusamy, Z. Aytac, and T. Uyar, Grain boundary engineering in electrospun ZnO nanostructures as promising photocatalysts, CrystEngComm **18**, 6341 (2016).
[14] C. Lops, A. Ancona, K. Di Cesare, B. Dumontel, N. Garino, G. Canavese, S. Hérnandez, and V. Cauda, Sonophotocatalytic degradation mechanisms of Rhodamine B dye via radicals generation by micro-and nano-particles of ZnO, Appl. Catal. B **243**, 629 (2019).
[15] C. Banning, J. Votteler, D. Hoffmann, H. Koppensteiner, M. Warmer, R. Reimer, F. Kirchhoff, U. Schubert, J. Hauber, and M. Schindler, A flow cytometry-based FRET assay to identify and analyse protein-protein interactions in living cells, PLoS ONE **5**, e9344 (2010).
[16] W. R. Algar, N. Hildebrandt, S. S. Vogel, and I. L. Medintz, FRET as a biomolecular research tool—Understanding its potential while avoiding pitfalls, Nat. Methods **16**, 815 (2019).
[17] S. Nadupalli, S. Repp, S. Weber, and E. Erdem, About defect phenomena in ZnO nanocrystals, Nanoscale **13**, 9160 (2021).
[18] E. Ebrahimi, M. Irfan, F. Shabani, Y. Kocak, B. Karakurt, E. Erdem, H. V. Demir, and E. Ozensoy, Core-crown quantum nanoplatelets with favorable type-II heterojunctions boost charge separation and photocatalytic NO oxidation on TiO_2, ChemCatChem **12**, 6329 (2020).
[19] V. Dybbert, S. M. Fehr, F. Klein, A. Schaadt, A. Hoffmann, E. Frei, E. Erdem, T. Ludwig, H. Hillebrecht, and I. Krossing, Oxidative fluorination of Cu/ZnO methanol catalysts, Angew. Chem. **131**, 13069 (2019).
[20] S. Repp and E. Erdem, Controlling the exciton energy of zinc oxide (ZnO) quantum dots by changing the confinement conditions, Spectrochim. Acta Part A **152**, 637 (2016).
[21] S. K. S. Parashar, B. S. Murty, S. Repp, S. Weber, and E. Erdem, Investigation of intrinsic defects in core-shell structured ZnO nanocrystals, J. Appl. Phys. **111**, 113712 (2012).
[22] V. Polshettiwar and R. S. Varma, Green chemistry by nano-catalysis, Green Chem. **12**, 743 (2010).
[23] K. Mondal and A. Sharma, Recent advances in the synthesis and application of photocatalytic metal–metal oxide core–shell nanoparticles for environmental remediation and their recycling process, RSC Adv. **6**, 83589 (2016).
[24] P. Rai, S. M. Majhi, Y.-T. Yu, and J.-H. Lee, Noble metal@ metal oxide semiconductor core@ shell nano-architectures as a new platform for gas sensor applications, RSC Adv. **5**, 76229 (2015).
[25] Y. Sun, L. Chen, Y. Bao, Y. Zhang, J. Wang, M. Fu, J. Wu, and D. Ye, The applications of morphology controlled ZnO in catalysis, Catalysts **6**, 188 (2016).
[26] H. Zou, Z. Luo, X. Yang, Q. Xie, and Y. Zhou, Toward emerging applications using core–shell nanostructured materials: A review, J. Mater. Sci. **57**, 10912 (2022).
[27] A. Mudhoo, S. Paliya, P. Goswami, M. Singh, G. Lofrano, M. Carotenuto, F. Carraturo, G. Libralato, M. Guida, M. Usman *et al.*, Fabrication, functionalization and performance of doped photocatalysts for dye degradation and mineralization: A review, Environ. Chem. Lett. **18**, 1825 (2020).
[28] M. Ahmad, E. Ahmed, Z. L. Hong, W. Ahmed, A. Elhissi, and N. R. Khalid, Photocatalytic, sonocatalytic and sonophotocatalytic degradation of Rhodamine B using ZnO/CnTs composites photocatalysts, Ultrason. Sonochem. **21**, 761 (2014).
[29] A. Janotti and C. G. Van de Walle, Fundamentals of zinc oxide as a semiconductor, Rep. Prog. Phys. **72**, 126501 (2009).
[30] K. Byrappa, A. K. Subramani, S. Ananda, K. M. L. Rai, R. Dinesh, and M. Yoshimura, Photocatalytic degradation of Rhodamine B dye using hydrothermally synthesized ZnO, Bull. Mater. Sci. **29**, 433 (2006).
[31] S. Parvaz, M. Rabbani, and R. Rahimi, Fabrication of novel magnetic ZnO hollow spheres/pumice nanocomposites for photodegradation of Rhodamine B under visible light irradiation, Mater. Sci. Engineer. B **263**, 114863 (2021).
[32] S. Stoll and D. Goldfarb, *EPR Spectroscopy: Fundamentals and Methods* (Wiley, United Kingdom, 2018).
[33] S. Stoll and A. Schweiger, EasySpin, a comprehensive software package for spectral simulation and analysis in EPR, J. Magn. Reson. **178**, 42 (2006).
[34] E. Duin, Short-short introduction to EPR spectroscopy, https://webhome.auburn.edu/~duinedu/epr/1_theory.pdf.
[35] M. H. Aleinawi, A. U. Ammar, M. Buldu-Akturk, N. S. Turhan, S. Nadupalli, and E. Erdem, Spectroscopic probing of Mn-doped ZnO nanowires synthesized via a microwave-assisted route, J. Phys. Chem. C **126**, 4229 (2022).
[36] K. Vanheusden, C. H. Seager, W. L. Warren, D. R. Tallant, and J. A. Voigt, Correlation between photoluminescence and oxygen vacancies in ZnO phosphors, Appl. Phys. Lett. **68**, 403 (1996).
[37] G. I. Cristina and M. Marazzi, *Theoretical and Computational Photochemistry: Fundamentals, Methods, Applications and Synergy with Experimental Approaches* (Elsevier, The Netherlands, 2023).
[38] J. E. Stehr, S. L. Chen, N. K. Reddy, C. W. Tu, W. M. Chen, and I. A. Buyanova, Turning ZnO into an efficient energy upconversion material by defect engineering, Adv. Funct. Mater. **24**, 3760 (2014).
[39] A. Artesani, M. V. Dozzi, L. Toniolo, G. Valentini, and D. Comelli, Experimental study on the link between optical emission, crystal defects and photocatalytic activity of artist pigments based on zinc oxide, Minerals **10**, 1129 (2020).

[40] Q. I. Rahman, M. Ahmad, S. K. Misra, and M. Lohani, Effective photocatalytic degradation of Rhodamine B dye by ZnO nanoparticles, Mater. Lett. **91**, 170 (2013).

[41] Z. Q. Bai and Z. W. Liu, A broadband photodetector based on Rhodamine B-sensitized ZnO nanowires film, Sci. Rep. **7**, 11384 (2017).

[42] G. A. Beane, A. J. Morfa, A. M. Funston, and P. Mulvaney, Defect-mediated energy transfer between ZnO nanocrystals and a conjugated dye, J. Phys. Chem. C **116**, 3305 (2012).

[43] H. Kirchberg, M. Thorwart, and A. Nitzan, Charge transfer through redox molecular junctions in nonequilibrated solvents, J. Phys. Chem. Lett. **11**, 1729 (2020).

[44] A. Nitzan, Polariton chemistry webinars: Confined emitters: Interference, electron transfer, and vibrational strong coupling, https://www.youtube.com/watch?v=aENinrgkwuw.

Correction: The second grant number in the first sentence of the Acknowledgment section was incorrect and has been fixed.